



The effect of shallow water bathymetry on swash and surf zone modeled by SWASH

Juliana Franco Lima ^{a,*}, Leandro Farina ^b, Pedro Veras Guimarães ^c, Ana Flávia Caetano Bastos ^d, Pedro de Souza Pereira ^d, Mauro Michelena Andrade ^e

^a Institute of Geosciences, Federal University of Rio Grande do Sul, Av. Bento Gonçalves, 9500, Porto Alegre, 91501-970, Rio Grande do Sul, Brazil

^b Institute of Mathematics and Statistics, Federal University of Rio Grande do Sul, Av. Bento Gonçalves, 9500, Porto Alegre, 91501-970, Rio Grande do Sul, Brazil

^c Department of Mechanical Engineering, Federal University of Santa Catarina, Eng. Agrônomo Andrey Cristian Ferreira Street, Florianópolis, 88.040-900, Santa Catarina, Brazil

^d Graduate Program in Oceanography, Federal University of Santa Catarina, Eng. Agrônomo Andrey Cristian Ferreira Street, Florianópolis, 88.040-900, Santa Catarina, Brazil

^e Polytechnic School, University of Vale do Itajaí, Uruguai Street, 458, Itajaí, 88302-901, Santa Catarina, Brazil

ARTICLE INFO

Keywords:

Wave model
Wave runup
Surf zone
Beach profile
Unmanned aerial vehicle bathymetry

ABSTRACT

Submerged topography in shallow waters is fundamental in the propagation and dissipation of ocean waves in the surf and swash zones. However, obtaining accurate bathymetric data in this region is challenging due to the high temporal and spatial environmental variability. The bottom boundary condition can directly affect the accuracy of numerical models used for shallow water simulations. In this study, the performance of the SWASH numerical model in describing wave runup in the swash zone is assessed using different bathymetric boundary conditions. The first method involves using data measured in the surf zone obtained by a Unmanned Aerial Vehicle (UAV), and analyzing it using the cBathy algorithm. The second method utilizes a regular bathymetric mesh generated from Dean's equilibrium profile combined with beach topography data. The third method relies exclusively on interpolation methods using data from deep waters and beach profiles. This interpolation approach is the most used among SWASH users when detailed or updated surf zone bathymetry is unavailable. Based on the numerical simulations performed, not incorporating data from the surf zone resulted in a 4% increase in the runup estimated and approximately a 2% difference in identifying the swash zone position. The method to obtain bathymetry through the cBathy algorithm, used in this article, is cost-effective and can be used to reduce uncertainties in surf zone numerical simulations, induced by the lack of knowledge about the bottom conditions.

1. Introduction

Wave runup refers to the maximum vertical height of seawater measured over the beach face, which is the sum of two parameters: swash and wave setup (Holman, 1986). Swash is defined as the fluctuations in the mean water level over the beach face, while wave setup is the superlevation of that level caused by wave breaking on the coast (Stockdon et al., 2006). Together, these parameters contribute to the overall height of the wave runup, which is an important factor in understanding the impact of ocean waves on coastal regions (Ruggiero et al., 2004).

The swash zone is a highly dynamic region that determines the morphological changes of beaches and may be responsible for adding

or removing sediment from the beach face (Bertin et al., 2017). Understanding the runup and swash dynamics becomes especially important during extreme events when there is a considerable increase in the wave setup, which can generate impacts and risks to coastal structures, such as accidents and loss of frontal dunes, and loss of anthropic structures (Guimarães et al., 2015; Medellín et al., 2016; Harley, 2017).

Based on parameterizations, using field analyses of wave statistical parameters and the beach slope, Stockdon et al. (2006) defined the 2% maximum exceedance of the wave runup, considering the slope of the sandy beaches, as

$$R_2 = 1.1 \left(0.35\beta_f (H_o L_o)^{\frac{1}{2}} \frac{[H_o L_o (0.563\beta_f^2 + 0.004)^{\frac{1}{2}}]}{2} \right), \quad (1)$$

* Corresponding author.

E-mail addresses: franjojuliana987@gmail.com (J.F. Lima), farina@alum.mit.edu (L. Farina), pedro.veras.guimaraes@ufsc.br (P.V. Guimarães), anafcb95@gmail.com (A.F.C. Bastos), pedro.s.pereira@ufsc.br (P. de Souza Pereira), mauromichelena@gmail.com (M.M. Andrade).

<https://doi.org/10.1016/j.ocemod.2024.102440>

Received 21 December 2023; Received in revised form 23 August 2024; Accepted 5 September 2024

Available online 7 September 2024

1463-5003/© 2024 Elsevier Ltd. All rights are reserved, including those for text and data mining, AI training, and similar technologies.

where H_o e L_o are the wave height and wavelength in deep water, respectively, and β_f is the foreshore beach slope. The beach slope is essential for the definition of R_2 (Lange et al., 2022). In addition to this, other parameterizations were obtained by using and reformulating the calculation of wave runup from empirical models and always considering the profile slope as a determining factor (Senechal et al., 2011b; Cox et al., 2013; Holman et al., 2014; Didier et al., 2020; Gomes da Silva et al., 2020).

More recent studies have been analyzing the risks of coastal flooding and the effects of storms on the coast through numerical wave models by taking into account the wave runup exceedance values (e.g., Guimarães et al., 2015; Nicolae Lerma et al., 2016; Medellín et al., 2016; Nicolae Lerma et al., 2017; Valentini et al., 2019; de Lima et al., 2020; Castelle et al., 2021; Stokes et al., 2021; Rutten et al., 2021; Henderson et al., 2022).

One approach often used to numerically investigate the processes that occur within the surf and swash zone is through the SWASH model (Simulating WAve till SHore Zijlema et al., 2011). This model uses the Shallow Water Non-Hydrostatic Equation to predict the behavior of the free surface. The accuracy of this approach strongly depends on the interaction between waves and the bathymetry of the surf zone, as well as the beach profile.

To evaluate the runup during storm events, Guimarães et al. (2015) carried out simulations with the SWASH model. In their study, bathymetric data was obtained in intermediate waters outside the surf zone, which were then interpolated along with altimetric data obtained from LIDAR scans of the surface land. However, this approach creates a data gap in the surf zone where no data is available. Furthermore, the collection of bathymetric data was conducted on different dates than the simulated experiments, potentially introducing errors in the model's predictions of runup and inundation.

On the other hand, Nicolae Lerma et al. (2017) employed remote sensing and in situ measurements to obtain more complex bathymetries for running the SWASH model in both 1D and 2D modes. To understand and accurately simulate the dynamics of wave setup and runup during storm conditions on beaches through complex morphologies, Nicolae Lerma et al. (2017) used topo-bathymetric data collected by Senechal et al. (2011a) during a storm at the same location and time period as their study. Measurements in situ and remote sensing were used to obtain topographic and bathymetric data (Senechal et al., 2011a). Daily topographic surveys were conducted using a GPS-equipped ATV in the dry areas, while in moderate water depths, these were performed by walking along the coast. Senechal et al. (2011a) used a video system (Cam-Era-NIWA technology) to acquire images with two cameras deployed on a foredune. The images were subsequently processed following the methodology of Almar et al. (2010), using satellite images for details of sub-tidal and inter-tidal bar systems.

Despite the importance of bathymetry in coastal processes, most of the previously mentioned studies (e.g., Guimarães et al., 2015; de Lima et al., 2020; Castelle et al., 2021; Stokes et al., 2021; Rutten et al., 2021) did not use realistic bathymetry of the surf zone. Instead, they relied only on deep water bathymetry, beach profiles, and interpolation to create the numerical grid. Moreover, these studies typically applied this approach to simulate various wave scenarios, often using bathymetry data collected during different periods.

To evaluate the interaction between waves and bathymetry, field experiments typically involve gathering data from topographic profiles, LIDAR scans, nautical charts, and high-frequency sensors or global positioning systems (GPS) (Holman, 1986; Ruggiero et al., 2004; Stockdon et al., 2006; Guimarães et al., 2015; Dodet et al., 2018; de Lima et al., 2020). However, obtaining accurate topographic and bathymetric data in the swash and surf zone is hampered by the high morphodynamic variability of this environment (Calliari et al., 2003).

To bridge the gap from deep and intermediate waters to shallow waters and surf zone bathymetries in numerical simulations, we investigated the use of Unmanned Aerial Vehicles (UAVs) equipped

with cameras. Studies by Holman et al. (2011, 2013, 2017), Vos (2017), Bergsma et al. (2019) utilized UAVs for remote observations and estimated bathymetries using the cBathy algorithm. This algorithm processes the captured video images and takes into account the wave dispersion relation (Eq. (2)) and the variation in water surface intensity to calculate depth data through inverse bathymetry (Holman et al., 2013). These studies assessed the precision of the method and identified limitations arising from instabilities and adverse weather conditions that can affect video capture.

Due to the highly dynamic nature of the surf zone, characterized by the frequent migration of sandbars, traditional geophysical methods face challenges in accurately measuring depths at high frequencies. As a result, the bathymetric data obtained using these methods may differ from the actual conditions (Rutten et al., 2021). Consequently, when using numerical modeling to predict wave runup, it is crucial to employ bathymetry collection methods that account for the dynamic nature of the surf zone and accurately describe the morphology during the specific period of the simulation (Vos, 2017; Nicolae Lerma et al., 2017; Valentini et al., 2019).

The primary aim of this study is to analyze and assess the SWASH model's performance in depicting wave runup and wave breaking zones using bathymetry obtained from UAV surveys. This evaluation involves three distinct bathymetric inputs: one derived from UAV data analyzed with the cBathy algorithm, another based on an Equilibrium Beach Profile (EBP), and the third from interpolation methods. The model's outputs is being compared with UAV-generated images to gauge its accuracy in representing sandbar positions and the runup line. Additionally, the study examines how variations in bathymetry influence wave runup simulated by the SWASH model, considering both realistic UAV-derived data and hypothetical bathymetry scenarios.

The paper is structured as follows: Section 2 introduces the Campeche Beach area, outlines the experimental setup, and explains the methods employed for generating bathymetric grids using UAVs, the cBathy algorithm, and Dean's profile. Section 3 provides a comprehensive description of the SWASH model and its input parameters. In Section 4, the outputs from cBathy and the SWASH model are presented and analyzed. Lastly, Section 5 concludes the paper with final remarks and considerations.

2. Material and methods

2.1. Study area and data acquisition

The study area chosen for this experiment was Campeche Beach, situated in the state of Santa Catarina, southern Brazil. Campeche Beach is located in Florianópolis (Fig. 1) and is characterized as an intermediate beach (Klein et al., 2016). It features a longitudinal rhythmic sandbar, rip currents, and beach cusps (Silveira et al., 2011). Additionally, Fig. 1D shows Campeche Island to the southeast of the study area, which is also within the computational domain used in this study.

According to Klein et al. (2016) the wave regime along the coast of Florianópolis exhibits a seasonal variation, with multi-modal seas occurring more frequently during the summer and less frequently during the winter. In the region, bimodal seas also display a well-defined seasonal variation, characterized by sea wind with a period of 8 s coming from the east and an average significant wave height (H_s) of 1.25 m (spring and summer). In addition, swell waves with a period of 12 seconds originate from the south and exhibit an increasing H_s from summer to winter, ranging from 1.25 m to 2 m and, although uncommon, significant wave heights exceeding 4 m can occur in all seasons (Araujo et al., 2003; Klein et al., 2016).

During the experiment, an ADCP (Acoustic Doppler Current Profiler), model Aquadopp 1 MHz, was moored at 18 m depth, from April 31 to May 5, 2019 (see Table 1). The ADCP was located approximately 800 m from the coast at coordinates 48.468777°W and 27.672539°S in longitude and latitude, as shown in Fig. 1D. The ADCP acquired various

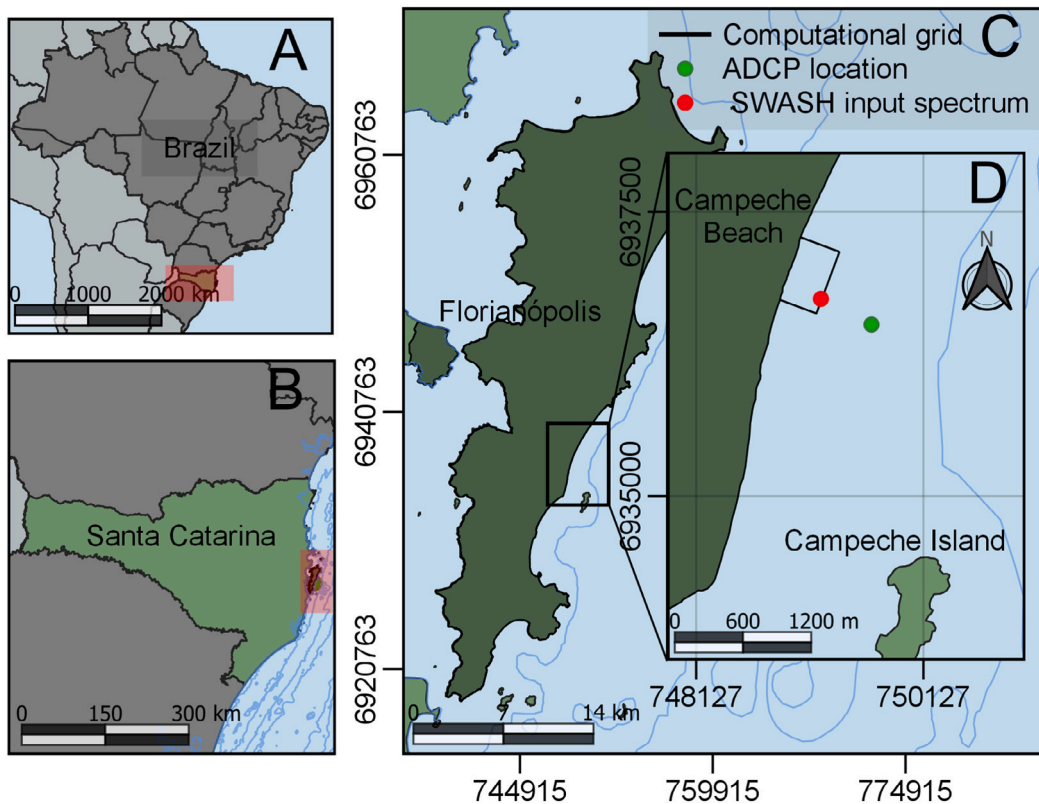


Fig. 1. (A, B and C) Map depicting the study area located in the southeast of Florianópolis city, Santa Catarina state, Brazil. (D) Campeche Beach, where field data was collected. The red dot marks the input location of the wave spectrum on the computational grid (black square), while the green dot indicates the ADCP location. Datum: SIRGAS 2000/ UTM zone 22 J.

wave parameters, vertical currents profiles and sea level measurements. However, for the purposes of the analysis, only water level, and wave spectrum were considered. The measured wave spectrum served as a boundary condition in the SWASH model, specifically inputted at the eastern edge of the computational grid (refer to Fig. 1D). The coordinates chosen for setting the spectral boundary conditions in the SWASH model were approximately 48.473271° W and 27.670582° S, situated approximately 300 m offshore. Both positions can be considered in intermediate water, given the wave conditions observed during the experiment. The SWASH computational grid did not extend to the location of the ADCP due to the lack of bathymetric data in this region.

The experiment was carried out under average wave conditions, often observed in the region. The dominant direction of the wave spectrum was east and southeast, with wave heights of approximately 1.5 m and a peak period of 8 s.

To measure beach and surf zone morphology, two different approaches were employed. The beach morphology was measured on April 27th, 2019, by surveying the beach topography using a TRIMBLE RTK R6 GPS receiver. The survey lines were established perpendicular to the coast and approximately 50 m apart from each other. For the surf zone morphology, video processing techniques were utilized, on the same day as the topographic data collection. A total of 17 min of video footage was captured using a DJI Mavic Pro Model, which is a quadcopter UAV (Unmanned Aerial Vehicle). The UAV was positioned in a stationary manner to ensure consistent data collection and minimize camera motion. The videos were recorded in 4K format with a resolution of 3840×2160 pixels.

Once the videos were collected, the images underwent processing to generate long exposure images and extract bathymetric information using the cBathy algorithm. The details of the cBathy algorithm will be elaborated in the following subsection, specifically in Section 2.2.

2.2. Inverse bathymetry estimation

To convert image data into bathymetric data, the first step is image rectification. This process converts oblique images captured by the UAV into flattened and scaled images with a metric scale, enabling the identification and positioning of morphological features (Holland et al., 1997). The resulting images allow for automated tracking of wave trajectories.

The bathymetric grid was generated from these images by using the cBathy algorithm, which is an algorithm that utilizes observations of surface wave light reflection patterns to estimate bathymetry data (Holman and Haller, 2013).

The dispersion relation used by the cBathy algorithm, as described by Dean and Dalrymple (1991), is given by:

$$\sigma^2 = gk \tanh(kh), \quad (2)$$

where, σ is the radial frequency (2π divided by the period T), k the radial wave number (2π divided by the wavelength, L), g the acceleration due to gravity and h the water depth.

To obtain bathymetry using the cBathy algorithm, three steps are needed (Holman et al., 2013; Bruder and Brodie, 2020). In stage 1 of the cBathy algorithm, the optical intensity time series for each pixel is Fourier transformed, providing wave number and frequency estimates. Using these wave numbers and frequencies, an equivalent water depth is estimated based on the dispersion relation. Additionally, a depth correction for the tidal stage is applied. This stage aims to estimate the depth-dependent properties of the waves observed in the video footage.

In stage 2 of the cBathy algorithm, the depth estimates obtained from stage 1 are combined to generate a single depth estimation for each point, along with error information. The algorithm seeks to find the depth value that provides the best fit between the observed frequency-wave number information and the dispersion relation. It is

important to note that the depths obtained in both stage 1 and stage 2 of the cBathy algorithm need to be corrected for tidal variations to obtain bathymetric data referenced to the tidal datum. This ensures consistency and accuracy in the resulting bathymetry data.

The objective of the stage 3 analysis is to calculate a running average that smooths the individual hourly estimates in a way that weighs the confidence in the new estimations relative to the previous running average. The Kalman filter is applied at this stage, which is a method detailed in Kalman (1960). Validation and evaluation of the cBathy algorithm, in terms of how it accurately describes and defines features in the areas closest to a beach, can be found in Holman et al. (2013), Vos (2017) and Brodie et al. (2018).

After completing the three stages of the cBathy algorithm, which provide bathymetric data for the Campeche beach area, the estimated bathymetry was interpolated along with the dry beach topographic data. In this study, a bathymetric grid with dimensions of 260m width and 341m length, with a spatial resolution of 1.5 m in the x direction and 1.7 m in the y direction, was generated.

2.3. Post-processing imagery

As a by-product of the rectified aerial images, the *timex*, which is a time average image of the light intensity, can also be obtained. A high contrast *timex* image, in which wave breaking foam coverage and darker pixels at the sea surface can be distinguished, allows us to identify the average wave breaking position and scattering.

The wave runup cross-shore variation changes the shoreline position over time and using the timestack we can capture this alteration. The timestack is created by combining sequential images or data frames taken at different time intervals or in a specific period, to represent the maximum and minimum cross-shore position along the shore. It is known as the “wave runup timestack” or “runup pixel stack” and is another important output obtained from the image rectification process (Holland et al., 1995). This timestack provides information about the maximum and minimum positions of the wave runup line at different times. It is a valuable dataset that can be used to validate the results of our model. To visualize and analyze the maxima and minima of the wave runup, an advanced automated edge detection routine was applied. This routine utilizes the *runupTool* (Vousdoukas et al., 2012), a specialized tool described in CIRN (2022), to highlight the position of the runup limit in the timestack.

2.4. Equilibrium beach profile and data interpolation

To evaluate potential errors arising from the use of theoretical bathymetry in the SWASH model and a lack of bathymetric data, two theoretical bathymetries were created based on the equilibrium profile concepts (EBP) of Dean (1991, 1997), derived from Bruun (1954).

Dean (1991) considered a theoretical profile using grain diameters. Consequently, this approach allows for the estimation of a beach profile based on the sedimentological and hydrodynamic characteristics operating at the site. Through laboratory analysis Dean (1991) proposed a beach equilibrium profile given by

$$h = Ay^{\frac{2}{3}}, \quad (3)$$

where h is the water depth at a seaward distance y from the shoreline and A is a scale parameter that depends primarily on sediment characteristics. There are several ways to calculate A (Komar, 1997), which usually provide values that vary between 0.2 and 1.2. According to Dean (1991),

$$A = \left[\frac{24D_*(D)}{5\rho g^{\frac{3}{2}}\kappa^2} \right]^{\frac{2}{3}}, \quad (4)$$

where D_* is uniform wave energy dissipation per unit volume in the break zone, which depends on sediment particle diameter D , ρ is the

water mass density, g is gravity and κ is a constant relating wave height to water depth within the surf zone. The profile slope has been considered in studies to estimate wave runup and it is an important factor in estimating wave runup (e.g., Stockdon et al., 2006; Yates et al., 2009; Holman et al., 2014; Matheen et al., 2021). In this study, grain diameters of 0.17 mm and 1.36 mm were utilized, as reported by Pazini et al. (2022). The profile length (y) corresponds to the extent of the bathymetric grid generated using the cBathy algorithm. Based on calculations by Komar (1997), the parameter A was determined to be approximately 0.15 and 0.23. The sub-aerial part of the beach profile uses the beach topography obtained from the RTK R6 GPS receiver. Fig. 2a illustrates a comparison of profiles obtained with $A = 0.15$ and $A = 0.23$. The Equilibrium Beach Profile (EBP) was then interpolated in two dimensions using topographic data from field surveys to derive a theoretical equilibrium profile for Campeche Beach with the same numerical grid dimensions (Fig. 2b, c, d).

Furthermore, previous works using SWASH do not use Dean's beach profile to estimate the surf zone morphology, instead they use only linear interpolation without surf zone bathymetry information (e.g., Guimarães et al., 2015). So we tested two interpolation methods for our dataset. One considered only linear interpolation from very deep waters utilizing bathymetric data from the SMC (2011), a Brazilian database, and the topography data from a field survey. The second method tested uses the same input data but was interpolated using the $v4$ method (Renka, 1988), (Fig. 2e). This is a bicubic interpolation technique used to smooth data in two dimensions. It is based on a multiquadric least squares interpolation method (Renka, 1988).

The SMC (2011) database comprises nautical charts and numerical models specifically designed for addressing issues within coastal zones. However, the bathymetry data in proximity to the study area exhibits a notably sparse density. Consequently, when applying linear interpolation using this data, it resulted in a bathymetry dataset with excessively shallow depths (ranging from 6m in the sub-aerial portion to 1m in depth at the eastern boundary limit), rendering it incompatible for processing with the SWASH model. Therefore, we are unable to present any results derived from this dataset here.

On the other hand, the $v4$ method produced a bathymetry profile ranging from over 5 m in the dry beach area to -20 m in the submerged portion (Fig. 2e). This profile exhibits a significantly steeper and unrealistic slope compared to the others. Nonetheless, these results will be presented here solely to discuss and bring attention to the model's sensitivity to synthetic surf zone profiles.

3. Numerical modeling in shallow water

The numerical approach was carried out using the non-hydrostatic model *Simulating Wave till SHore* (SWASH), governed by non-linear shallow water equations and capable of describing the mean depth and free surface flow, considering the conservation of mass and vertical momentum (Zijlema et al., 2011). The model is capable of accomplishing simulations in short and meso scale and can be applied in 1D and 2D modes. It is derived from the incompressible Navier–Stokes equations that comprise the conservation of mass and momentum (Eqs. (5)–(7)).

$$\frac{\partial \zeta}{\partial t} + \frac{\partial hu}{\partial x} + \frac{\partial hv}{\partial y} = 0 \quad (5)$$

$$\frac{\partial u}{\partial t} + u \frac{\partial u}{\partial x} + v \frac{\partial u}{\partial y} + \frac{1}{h} \int_{-d}^{\zeta} \frac{\partial q}{\partial x} dz + c_f \frac{u\sqrt{u^2 + v^2}}{h} = \frac{1}{h} \left(\frac{\partial h\tau_{xx}}{\partial x} + \frac{\partial h\tau_{xy}}{\partial y} \right) \quad (6)$$

$$\frac{\partial v}{\partial t} + u \frac{\partial v}{\partial x} + v \frac{\partial v}{\partial y} + \frac{1}{h} \int_{-d}^{\zeta} \frac{\partial q}{\partial y} dz + c_f \frac{v\sqrt{u^2 + v^2}}{h} = \frac{1}{h} \left(\frac{\partial h\tau_{yx}}{\partial x} + \frac{\partial h\tau_{yy}}{\partial y} \right) \quad (7)$$

where t is the time, x and y are located at the still water level, and the z -axis points upwards. $\zeta(x, y, t)$ is the surface elevation measured from the still water level, $d(x, y)$ is the still water depth or the downward measured bottom level, $h = \zeta + d$ is the water depth, or total depth, $u(x, y, t)$ and $v(x, y, t)$ are the depth-averaged flow velocities in x - and

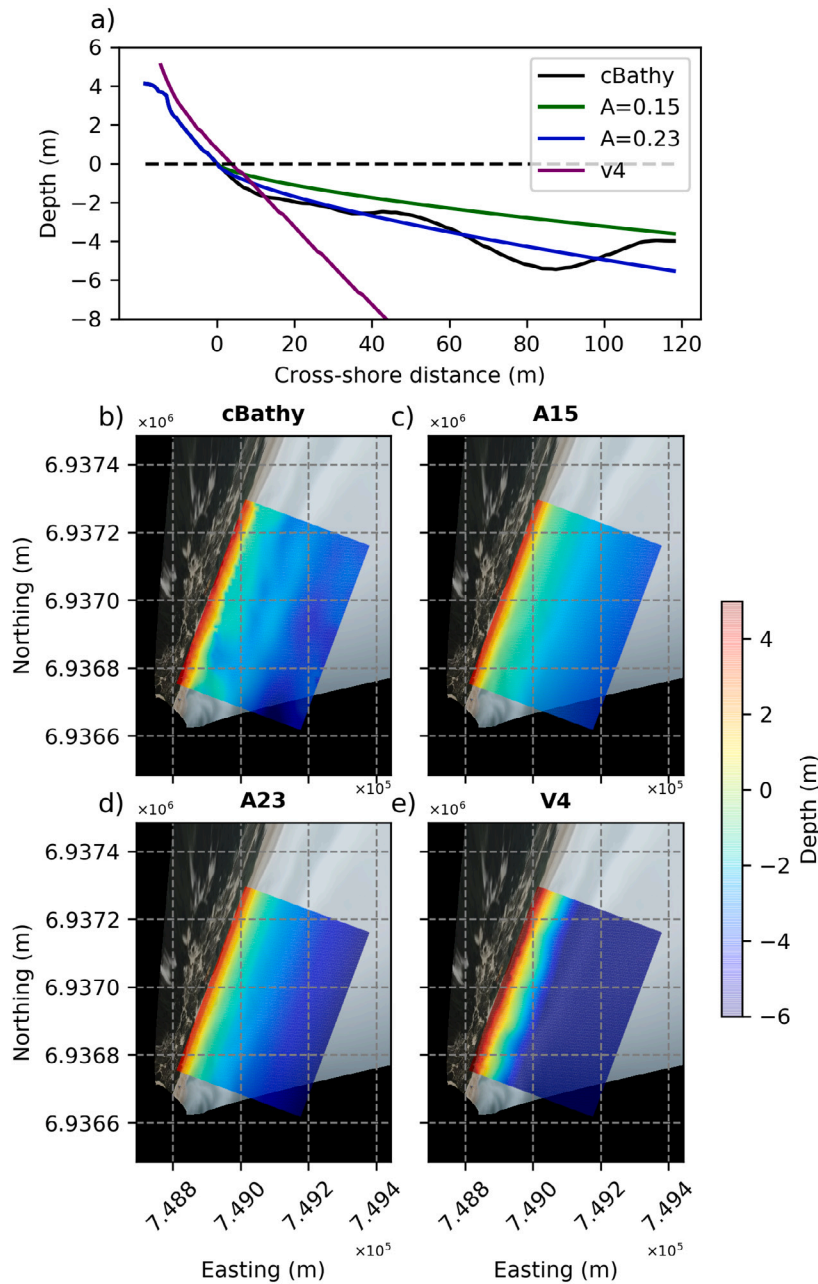


Fig. 2. (a) Equilibrium profiles according to Dean’s equation with $A = 0.15$ and $A = 0.23$, compared to the selected profile of the bathymetric grid generated by the cBathy algorithm and the v4 grid. Plan view of bathymetry generated by the cBathy algorithm (b), and bathymetries generated by the equilibrium profiles with $A = 0.15$ (c) and $A = 0.23$ (d), as well as bathymetry interpolated with v4 (e).

y -directions, respectively. $q(x, y, z, t)$ is the non-hydrostatic pressure (normalized by the density), g is the gravitational acceleration, c_f is the dimensionless bottom friction coefficient, and τ_{xx} , τ_{xy} , τ_{yx} and τ_{yy} are the horizontal turbulent stress terms.

The numerical simulations were run to simulate the surf and swash zone processes at 5 different moments of the field experiment, as outlined in Table 1. In the model, the **initial turbulence** was set to zero using SWASH’s commands. Additionally, commands such as **breaking** were employed to control the wave breaking, **viscosity** to account for turbulent mixing, and **friction** to activate the bottom friction in modeling process. The wave spectrum for each simulation was obtained from the ADCP data at the corresponding time using wave energy and directional spectra information, and the sea surface high was adjusted based on the start time of each simulation. A spin-up time of 5 min was used, with a time step of 0.001 s, with the model outputs recorded

at a time interval of 1 s. The default maximum 0.8 and minimum 0.4 Courant numbers for automatic times step control were used in the simulation and the minimum depth for computation was set to 0.005 m. The total simulation time was 22 min, which included a 5-minute spin-up period. The subsequent 17 min were dedicated to analysis. This simulation duration was aligned with the duration of the UAV flight, which lasted 17 min. Further details for each simulation are presented in Table 1.

To evaluate the variation of wave runup and wave breaking, output data was generated for the bottom level, horizontal runup, water level, and wave breaking. The runup and wave breaking outputs from SWASH are represented by binary matrices, in which a value of 0 indicated the absence of runup or wave breaking, and a value of 1 indicated the presence of runup or active wave breaking at a specific location. These binary matrices provided a clear representation of the spatial

Table 1
The simulations details and wave parameters from the ADCP utilized in the simulations.

Simulation scenarios	Starting time (am)	Water level (m)	Significant height (m)	Peak period (s)
01	08:00	0.45 m	1.58	7.81
02	08:30	0.47 m	1.50	8.20
03	09:30	0.42 m	1.58	7.79
04	10:00	0.45 m	1.51	8.03
05	11:20	0.44 m	1.45	8.04

distribution of runup and wave breaking throughout the simulation domain.

The matrix generated for the wave runup contains the average of the maximum values of that variable across the dataset, resulting in a single matrix. In this matrix, a value of 0 indicates dry zones where wave runup does not occur, while a value of 1 indicates wet zones where wave runup is present. For wave breaking, a separate matrix is generated for each simulation time step. Each matrix represents the positions where wave breaking occurs during that specific time step. Similar to the wave runup matrix, a value of 1 in the wave breaking matrix indicates that the wave is breaking at that particular location and time, while a value of 0 indicates the absence of wave breaking.

The runup maximum point in the binary matrix was identified for each simulation along the profile. To determine the vertical runup height at this point, with respect to the still water level, the corresponding value of the bottom level output (*bot*) from the SWASH simulations was obtained. At locations where the initial runup was zero, the bottom level, or still water depth, is measured vertically from the water surface to the bottom, multiplying it by -1 gives the runup height value. Therefore, the vertical runup height at the maximum runup point is calculated as $bot \times -1$. This provides a measure of how much the wave has elevated above the surface of the water at that specific location.

In the results obtained from SWASH for wave runup, the Sobel edge detection filter was applied to enhance the visualization of the wave runup peaks along the coastline (Virtanen et al., 2020). The Sobel filter is a commonly used image processing technique that emphasizes edges in an image by calculating the gradient magnitude. By applying this filter, noise effects are reduced, and the prominent peaks of the wave runup are highlighted. The filter identifies these points based on the matrix values of the image and extracts them, making it easier to analyze and interpret the wave runup patterns (Kanopoulos et al., 1988; Gao et al., 2010; Ma et al., 2010). The SWASH model results were compared to the corresponding maximum wave runup point obtained using the *runuptoolbox* (Vousdoukas et al., 2012) from the UAV data.

The wave breaking frequency (F_b) in this case was defined by the sum of the binary matrices obtained from the wave breaking output in SWASH (*brk*) divided by the total number of SWASH outputs (n_t), in which 1 represents the position of the grid points where breaking is occurring and a value of 0 indicates areas where waves are not breaking. Thus,

$$F_b = \frac{\sum_{n=1}^{n_t} (brk)_n}{n_t} * 100, \quad (8)$$

where $n = 1$ is the first frame after the 5 min spin-up period, which was excluded from the analysis. This result can be qualitatively compared to the breaking position estimated from the UAV *timex* image.

4. Results and discussions

By using the *timex* images, it is possible to identify the wave breaking and scattering zone (e.g., Holland et al., 1997; Almar et al., 2010; Holman et al., 2013; Gomes et al., 2016; Vos, 2017). It is expected that the position of the breaking and swash zone corresponds to the numerical predictions from the SWASH model (Gomes et al., 2016).

The frequency of wave breaking for all the bathymetries simulated was superimposed on the *timex* image collected at the same time as the numerical experiment in Fig. 3. For the cBathy bathymetry, the

concentration of wave breaking frequency is observed in the regions of longitudinal sandbars, which is the same location observed by *timex*. As expected, a much higher frequency of wave breaking is observed in the swash zone than over the sandbars, with a reduction of this frequency in areas of longitudinal troughs and at greater depths (3a).

The SWASH model's wave breaking output provides the spatial and temporal occurrence of individual wave breaks. Analyzing wave breaking frequencies helps pinpoint areas where breaking occurs most frequently. Considering all the simulations, the highest observed breaking density exceeded 6% across all grid points, encompassing both breaking and non-breaking waves. This phenomenon predominantly manifests itself along the coastline, in the swash zone.

Besides the swash zone, the surf zone is expected to exhibit the second highest frequencies of wave breaking. Simulations using cBathy bathymetry indicated a wave breaking frequency of approximately 4% in the surf zone. The EBP model (A15) displayed varying wave breaking rates between 3% and 2% within both the surf zone and the eastern portion of the grid (Fig. 3b). In the Dean profile (A23) bathymetry, wave breaking begins shortly after the surf zone and continues uninterrupted until reaching the shoreline, where peak values were observed (Fig. 3c). In contrast, simulations using the V4 bathymetry, which features a steep beach profile, do not show a distinct surf zone, resulting in wave breaking predominantly occurring within the swash zone (Fig. 3d).

For intermediate beaches, wave breaking is expected to occur in the sand bank and dissipate most of the remaining energy in the swash zone. This was well reproduced by the model as depicted in Fig. 3a. On the other hand, the bathymetries generated using the EBP with a value of $A = 0.15$ and $A = 0.23$ do not have a good representation of the sandbar and exhibited a higher breaking frequency closer to the coast line, as illustrated in Fig. 3c, and 3d.

The distance from the swash zone to the first point where the waves break, as shown in the profile in Fig. 3a, was approximately 200 m, which corresponds to the first sandbar area in the cBathy grid. Moreover, some of the frequency breaking start in distances of 318 m occur near the eastern edge of the grid, before the first sandbar located in the surf zone.

In contrast, for $A = 0.23$, a clear sandbar is absent in the bottom profile. Consequently, the distance from the swash zone to the first wave breaking was around 150 m (Fig. 3c). On the other hand, the EBP bathymetry with $A = 0.15$ exhibits a shallower profile and without sandbars. Consequently, wave breaking commenced earlier and was more dispersed across the grid (Fig. 3b).

In the steep bathymetry generated using v4 interpolation, wave breaking mostly occurred just before the shoreline. There was little variation in wave breaking, with a 2% breaking frequency in the swash zone (Fig. 3d).

The foam coverage observed in the *timex* images is an indication of the breaking point position according to Holland et al. (1997). The values observed in the *timex* images (based on average pixel intensity) show that the waves also start to break around 200 m from the swash zone. The observed convergence of breaking wave positions with the numerical simulation using cBathy bathymetry can be explained by the fact that the *timex* data was used as input in the cBathy algorithm to generate the bathymetric grid, which, in turn, was used in the simulations by the SWASH model.

This result was anticipated, as demonstrated in a study conducted by Gomes et al. (2016), where a qualitative comparison was made

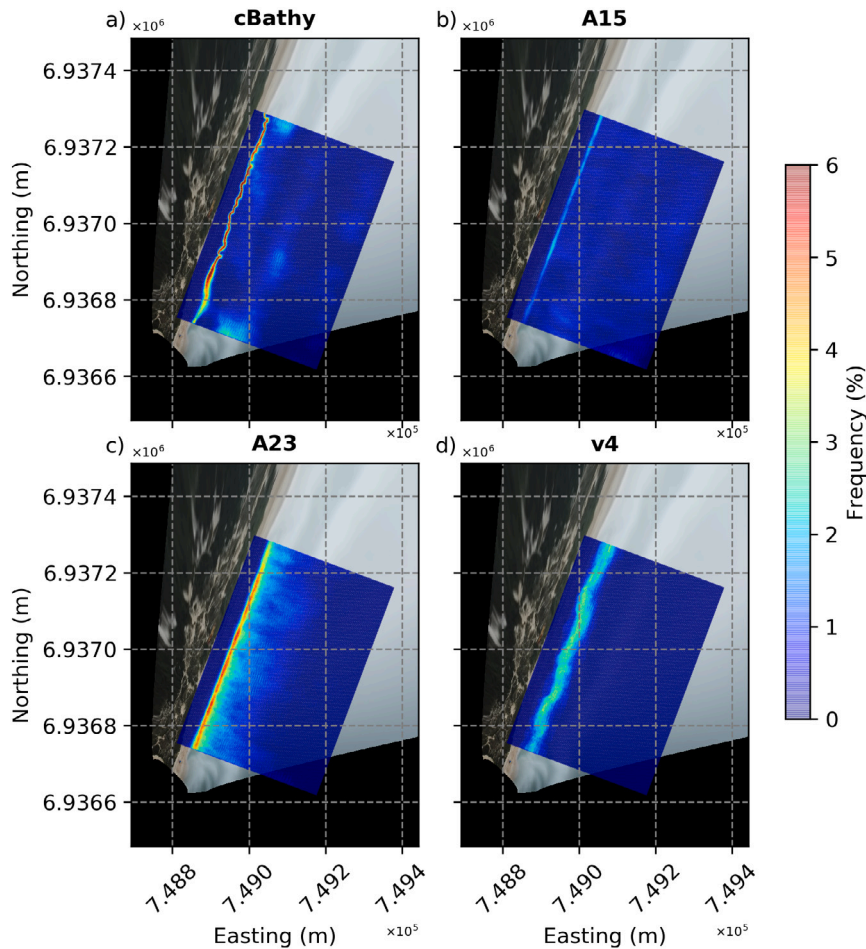


Fig. 3. Wave breaking frequency calculated from the SWASH results for each simulation performed for cBathy, EBP ($A = 0.15$ and $A = 0.23$) and v4 bathymetry, corresponding to the 3rd simulation (9:20 AM), superimposed on the observed *timex*.

between data generated by SWASH and observations from a video monitoring system (Argus imagery). In their study, Gomes et al. (2016) found that the SWASH model accurately predicted wave breaking locations compared to images captured by the Argus station. However, the images obtained by Gomes et al. (2016) were from a fixed remote monitoring system (Argus imagery), which, like UAVs, can be affected by wind or cloud interference. The accuracy estimated by Gomes et al. (2016) was about 1 m, approximately the same observed by Vos (2017) for UAVs.

Vos (2017) also observed, in his comparison study between the cBathy algorithm and a bathymetry obtained by sensors attached to jet skis, that the root mean square error between the bathymetries was on the scale of meters (between 1 and 2 m), in very shallow areas (below 3 m deep); while, in depths greater than 3 m, this value decreased to 50 cm. This occurs because the wave shape close to the breaking diverges from the linear dispersion relation, which is the basis for the cBathy algorithm (Holman et al., 2013).

Fig. 4 shows the average difference in the breaking frequency between the values obtained with cBathy and with EBP ($A = 0.15$ and $A = 0.23$) and bathymetry v4. This difference was computed for each of the 5 simulations and then averaged. The average difference observed between the bathymetric grids of cBathy and EBP A15 generates a difference of 4% approximately at 50 m in the cross-shore distance, and some positive differences where the longitudinal banks are located in the cBathy grid. Overall, all bathymetries exhibited a positive difference at this position, with the exception of grid A23 which becomes slightly negative at the first beach bank. Negative values indicate areas where the frequency of wave breaking is higher in simulations using

A15 and A23 bathymetries compared to the frequency observed with cBathy bathymetry. In the case of bathymetry A15, it exhibited low frequencies of breaking and, therefore, showed almost no difference compared to the cBathy bathymetry. These negative values of average difference match with the maxima intensity of frequency of breaking observed in the swash zone of each grid bathymetry. Overall, A15 provides a clearer representation of the wave breaking position between the first sandbar and the swash zone, while A23 accurately depicts the wave breaking position according to SWASH. In contrast, V4 shows the poorest representation and produces unrealistic results.

The legend of the Fig. 4 needs completion. Something like: (a) Graph of the average difference (%) in the wave breaking frequency between the values obtained with cBathy and with Dean's EBP ($A = 0.15$ and $A = 0.23$) and v4 (left-axis). The blue shaded area represents the cBathy profile with the cross-shore distance (x-axis) and the depth (right-axis) adjusted. And, (b), (c) and (d) are the plan view of the breaking line differences for EBP A15, EBP A23 and V4, respectively.

In Figs. 4b e 4c, it is possible to observe by the EBP, referring to the bathymetric grid of the cBathy, the two lines superimposed in the cBathy profile in the same cross-shore distance. And, with a plan view for A15 and A23, the average difference between the cBathy and EBP and the bathymetry v4. In the grid generated for the EBP, A23, this difference is more visible, with the break lines in the swash zone between the two grids.

It is notable that there is a trend of breaking in all the grids before the breaking line of the one generated by cBathy. However, this trend is more pronounced in the grid generated by the v4 interpolation indicating a higher occurrence of wave breaking at that location. It is

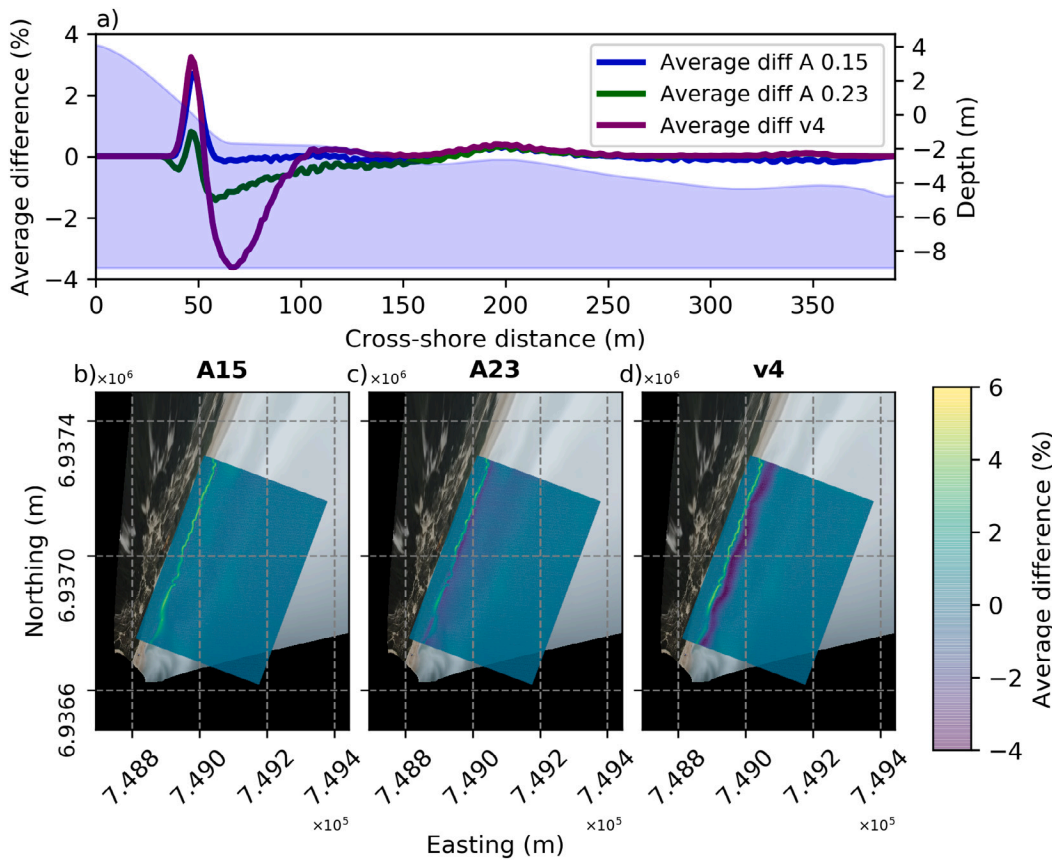


Fig. 4. Graph of the average difference in the wave breaking frequency between the values obtained with cBathy and with and Dean’s EBP ($A = 0.15$ and $A = 0.23$) and v4 (left axis). The blue shaded area represents the cBathy profile with the cross-shore distance (x-axis) and the depth (right-axis) adjusted. And, (b), (c) and (d) are the plan view of the breaking line differences for $EBPA_{15}$, $EBPA_{23}$ and v_4 , respectively.

also noticeable that there is a difference in the swash zone in the grid A23, approximately at 50 m in the cross-shore distance, where there is a small percentage of waves breaking at this location as well.

In Fig. 5, the point where the runup maxima were captured by the “runuptoolbox” (Vousdoukas et al., 2012) is represented by a blue line. There is a variation in the spread of the maximum and minimum points in the time stack, with a difference of approximately 12 m between different points. To validate the runup results, the values of maximum runup simulated from SWASH results were selected at the same location point obtained from the location captured by the “runuptoolbox” (Fig. 5). The values found using the bathymetries within SWASH are detailed in Table 2.

A comparison between the vertical wave runup elevation measured by the UAV *timestack* and the SWASH models outputs is presented in Table 2. The observed wave runup elevation (R_{obs}) was 1.21 m, from the *timestack* at approximately 9:30 am. This value is used as a reference to compare with the SWASH model results and was collected during the UAV flight. The simulations using the cBathy bathymetry condition ranged from 1.24 m to 1.56 m, corresponding to 10:00 am and 11:20 am, respectively, while the runup generated by the EBP with $A = 0.15$ were slightly lower, between 1.04 m to 1.17 m. However, the values from the bathymetry generated by $A = 0.23$ were closer to those obtained from the wave runup by cBathy, varying between 1.25 m and 1.54 m at 8:30 am and 9:30 am, respectively. Overall, the bathymetry generated by A23 was closer to and more similar to the cBathy bathymetry profile. This occurs because $A = 0.15$ produced smooth bathymetry gradients that emerged before $A = 0.23$ EBP (see Fig. 2), potentially altering the height and excursion of the wave runup.

The data obtained using the bathymetry through v4 interpolation presented values greater than all the simulations performed, varying

from 1.65 m up to 2.20 m at 11:20 am and 9:30 am, respectively. As it is a deeper bathymetry with a steeper slope in the sub-aerial part compared to the other bathymetries, resulting in more abrupt wave breaking, the wave runup results were higher than with the other methods. The topography and depth of the bathymetry directly influence the wave runup height, as observed in the results obtained with the bathymetry from the v4 interpolation method (Wright and Short, 1984).

The vertical wave runup heights from the grids generated by cBathy and EBP A23 overestimate slightly the vertical wave runup height observed on the day of data collection, which was 1.20 m. However, the height obtained by cBathy showed a smaller difference compared to the other grids (22 cm). On the other hand, the R_{A15} obtained by EBP A15 presented the smallest difference, being the bathymetry that best described the swash zone among all the other bathymetries. Nevertheless, this may be associated to the low slope of the bathymetry, which resulted in lower runup values in the simulations conducted with this bathymetry.

Despite the cBathy algorithm being known to present an error in the order of meters in the bathymetry around the breaking zone and centimeters in deeper waters (Holman et al., 2013), the algorithm was able to more accurately represent the features found on the bottom of Campeche Beach, in spite of the equilibrium profile being estimated with data and information from the beach.

It is noticeable that A15 did not perform well in representing the breaking location. However, it excelled in estimating the runup, outperforming both cBathy and A23 bathymetry. For the same sea state conditions, the wave energy dissipation rate in shallow water is mostly controlled by the sandbar positions and slope. The numerical simulation results using cBathy bathymetry show a slight tendency to

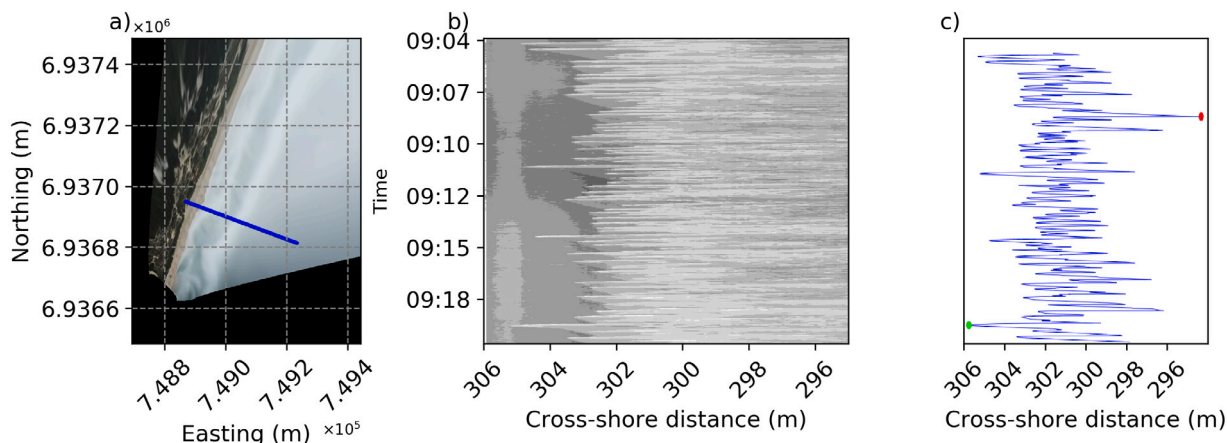


Fig. 5. Cross-shore transect (blue line) used for the analysis of swash data (a); timstack of wave runup showing time (y-axis) and cross-shore distance (x-axis) (b); and runup oscillation edges indicated by the maximum point (green dot), minimum point (red dot), and wave runup variation (blue line) (c).

Table 2

Maximum vertical wave runup height (R) between observed data (R_{obs}) from timstack image, and numerically simulated by SWASH using UAV subproducts (R_{cBathy}), and Dean profile with $A = 0.15(R_{A15})$ and $A = 0.23(R_{A23})$.

Simulation	Hour [AM]	R_{obs} [m]	R_{cBathy} [m]	R_{A15} [m]	R_{A23} [m]	R_{v4} [m]
01	08:00	–	1.39	1.04	1.39	1.90
02	08:30	–	1.53	1.12	1.25	1.75
03	09:30	1.21	1.42	1.17	1.54	2.20
04	10:00	–	1.24	1.04	1.39	1.90
05	11:20	–	1.56	1.05	1.40	1.65

overestimate the wave runup. In other words, the dissipation rate of the SWASH model might still need some adjustments. This was also observed in previous studies using bathymetries obtained by remote sensing (Nicolae Lerma et al., 2016; Valentini et al., 2019) and in other studies evaluating wave runup using the model (Medellin et al., 2016; Henderson et al., 2022).

Regardless of the numerical and physical uncertainties that may be present in the model, the absence of a reliable underwater topography and interpolation methods can often lead to incorrect results that are difficult to quantify. The use of the cBathy algorithm provides (when it is not possible to directly measure the bathymetry) much more reliable underwater morphology, which is essential for shallow water wave transformations and energy dissipation, than simplified empirical beach profiles or unknown interpolated features. In the absence of UAV or images to reconstruct the underwater beach profile, theoretical profiles, such as Dean’s, can provide much more realistic results than interpolation methods. In this paper, we demonstrate that generating a bathymetric grid through linear and v4 interpolation methods, under conditions of very limited measured data in intermediate waters, leads to highly unrealistic results when applied to the SWASH model. The primary issue is that the surf zone exhibits highly dynamic morphology. Consequently, relying on interpolation methods in areas where data is unavailable introduces significant, unquantified errors into the numerical simulations.

5. Conclusion

Numerical models used to detail shallow water processes are often limited by the availability of bathymetric data. The positioning and shape of the sandbar are essential for the dissipation and propagation of wave energy in shallow waters. Without sufficient detail, flood conditions may be under- or over-estimated. The problem is that the surf zone is a highly energetic and dynamic system, so directly estimating beach morphology is usually a challenging task.

This work examined an economical and non-invasive way to obtain bathymetric information in the surf zone. If compared to other traditional surveying methods, the system can be low-cost as it only requires

a 4 K quality UAV and a GPS-RTK to search ground control points. Data collection can be carried out even in stormy conditions, as long as safe flight conditions are met.

The numerical simulation with the SWASH model using EBP A15 better described the swash zone, and the wave runup values corresponded to those obtained in the field. However, when compared to the *timex* image, the breaking zone and swash zone locations were properly represented by the cBathy numerical simulations.

This discrepancy was related to the exponential-based beach profile described by Dean (1991), which lacks features such as sandbars and troughs, thus preventing waves from breaking and dissipating energy over these sandbars, possibly changing how waves arrive at the coast and consequently the wave runup height. It is unclear how the model would estimate wave runup height if features such as longitudinal bars with low slopes, which could dissipate wave energy, were included in the beach profile morphology.

During the data collection for bathymetry and topography information on Campeche Beach, the sediment grain size data for that day was not collected. The Pazini et al. (2022)’s values that were used in place of observed ones may have limited or altered the profile construction. Another limiting factor that prevented a deeper exploration of the statistical analyses of the present study was the lack of data regarding wave runup and wave breaking from Brazil and from dissipative beaches using bathymetry via remote methods. This hindered the discussion and comparisons that could have been made based on previously conducted studies.

Nevertheless, in terms of feature description, the simulations conducted using the cBathy bathymetry successfully described the location of the longitudinal sandbanks and the wave breaking occurring in this region, although they overestimated the wave runup value. Thus, an option for studies aimed at describing and focusing on the surf zone for the assessment of wave breaking and/or other processes occurring in this region.

Most of the previous studies employing the SWASH model have seldom included observed data in the breaking zone and often depend on interpolation between deep water to represent the shallow water

topography. This also tends to produce smoother or steeper bathymetries, depending on data density and the interpolation method. This may produce unknown errors in the numerical simulations since the bottom condition tends to vary based on data availability at different locations and sea state conditions.

This paper introduces a feasible alternative to a complete baseline condition for modeling coastal processes, taking into account potential errors and exploring alternative approaches to minimize them. Therefore, the present study suggests a simple method to improve numerical simulations in shallow water by providing more reliable bathymetry data. This can be essential for a better assessment of shallow water dynamics and provide more accurate data to improve the model parameterizations.

CRedit authorship contribution statement

Juliana Franco Lima: Writing – original draft, Visualization, Validation, Software, Methodology, Investigation, Formal analysis, Data curation, Conceptualization. **Leandro Farina:** Writing – review & editing, Supervision, Software, Investigation, Conceptualization. **Pedro Veras Guimarães:** Writing – review & editing, Supervision, Software, Investigation, Data curation, Conceptualization. **Ana Flávia Caetano Bastos:** Software, Methodology, Funding acquisition. **Pedro de Souza Pereira:** Writing – review & editing, Methodology, Funding acquisition. **Mauro Michelena Andrade:** Writing – review & editing, Funding acquisition.

Declaration of competing interest

The authors declare that they have no known competing financial interests or personal relationships that could have appeared to influence the work reported in this paper.

Data availability

Data will be made available on request.

Acknowledgments

J.F. Lima, would like to thank the Conselho Nacional de Desenvolvimento Científico e Tecnológico (CNPq) for the support as a scientific research fellow. The authors would like to thank the Graduate Program in Geosciences from the Federal University of Rio Grande do Sul (UFRGS) for the attention to the students during the pandemic. We also like to thank to Integrated Laboratory of Scientific Computation - LICC (PPGMap-UFRGS) for assisting with SWASH modeling simulations. P.S. Pereira, would like to thank CNPq for the financial support via the processes 311332/2022–6 and 425007/2016-2.

References

Almar, R., Castelle, B., Ruessink, B., Sénéchal, N., Bonneton, P., Marieu, V., 2010. Two- and three-dimensional double-sandbar system behaviour under intense wave forcing and a meso-macro tidal range. *Cont. Shelf Res.* 30 (7), 781–792. <http://dx.doi.org/10.1016/j.csr.2010.02.001>, URL <https://www.sciencedirect.com/science/article/pii/S0278434310000348>.

Araujo, C.E.S., Franco, D., Melo, E., Pimenta, F., 2003. Wave regime characteristics of the southern. In: *International Conference on Coastal and Port Engineering in Developing Countries*, no. 097. pp. 1–15.

Bergsma, E.W., Almar, R., Melo de Almeida, L.P., Sall, M., 2019. On the operational use of UAVs for video-derived bathymetry. *Coast. Eng.* 152, 103527. <http://dx.doi.org/10.1016/j.coastaleng.2019.103527>, URL <https://www.sciencedirect.com/science/article/pii/S0378383918303582>.

Bertin, X., Olabarrieta, M., McCall, R., 2017. Hydrodynamics under storm conditions. In: *Coastal Storms*. John Wiley and Sons, Ltd, pp. 23–43. <http://dx.doi.org/10.1002/9781118937099.ch2>, arXiv:<https://onlinelibrary.wiley.com/doi/pdf/10.1002/9781118937099.ch2>.

Brodie, K.L., Palmsten, M.L., Hesser, T.J., Dickhudt, P.J., Raubenheimer, B., Ladner, H., Elgar, S., 2018. Evaluation of video-based linear depth inversion performance and applications using altimeters and hydrographic surveys in a wide range of environmental conditions. *Coast. Eng.* 136, 147–160. <http://dx.doi.org/10.1016/j.coastaleng.2018.01.003>, URL <https://www.sciencedirect.com/science/article/pii/S0378383917301989>.

Bruder, B.L., Brodie, K.L., 2020. CIRN Quantitative Coastal imaging toolbox. *SoftwareX* 12, 100582. <http://dx.doi.org/10.1016/j.softx.2020.100582>, URL <https://www.sciencedirect.com/science/article/pii/S2352711020302958>.

Bruun, P., 1954. Coast erosion and the development of beach profiles. In: *US Army Corps of Engineers*, no. 44. p. 79.

Calliari, L.J., Muehc, D., Hoefel, F.G., Toldo, Jr., E., 2003. Morfodinâmica praias: uma breve revisão. *Revista Brasileira de Oceanografia* 51 (unico), 63–78. <http://dx.doi.org/10.1590/s1413-77392003000100007>.

Castelle, B., Masselink, G., Scott, T., Stokes, C., Konstantinou, A., Marieu, V., Bujan, S., 2021. Satellite-derived shoreline detection at a high-energy meso-macrotidal beach. *Geomorphology* 383, 107707. <http://dx.doi.org/10.1016/j.geomorph.2021.107707>, URL <https://www.sciencedirect.com/science/article/pii/S0169555X2100115X>.

CIRN, 2022. RunupTool-toolbox, coastal imaging research. <https://github.com/Coastal-Imaging-Research-Network/runupTool-Toolbox>.

Cox, N., Dunkin, L.M., Irish, J.L., 2013. An empirical model for infragravity swash on barred beaches. *Coast. Eng.* 81, 44–50. <http://dx.doi.org/10.1016/j.coastaleng.2013.06.008>, URL <https://www.sciencedirect.com/science/article/pii/S0378383913001178>.

de Lima, A., Khalid, A., Miesse, T.W., Cassalho, F., Ferreira, C., Scherer, M.E.G., Bonetti, J., 2020. Hydrodynamic and waves response during storm surges on the southern Brazilian coast: A hindcast study. *Water* 12 (12), <http://dx.doi.org/10.3390/w12123538>, URL <https://www.mdpi.com/2073-4441/12/12/3538>.

Dean, R.G., 1991. Equilibrium beach profiles: Characteristics and applications. *J. Coast. Res.* 7 (1), 53–84, URL <http://www.jstor.org/stable/4297805>.

Dean, R.G., 1997. Models for barrier island restoration. *J. Coast. Res.* 13 (3), 694–703.

Dean, R.G., Dalrymple, R.A., 1991. *Water Wave Mechanics for Engineers and Scientists*. World Scientific, <http://dx.doi.org/10.1142/1232>, arXiv:<https://www.worldscientific.com/doi/pdf/10.1142/1232>.

Didier, D., Caulet, C., Bandet, M., Bernatchez, P., Dumont, D., Augereau, E., Floc'h, F., Delacourt, C., 2020. Wave runup parameterization for sandy, gravel and platform beaches in a fetch-limited, large estuarine system. *Cont. Shelf Res.* 192, 104024. <http://dx.doi.org/10.1016/j.csr.2019.104024>, URL <https://www.sciencedirect.com/science/article/pii/S0278434319304078>.

Dodet, G., Leckler, F., Sous, D., Arduhin, F., Filipot, J., Suanes, S., 2018. Wave runup over steep rocky cliffs. *J. Geophys. Res.: Oceans* 123 (10), 7185–7205. <http://dx.doi.org/10.1029/2018JC013967>, arXiv:<https://agupubs.onlinelibrary.wiley.com/doi/pdf/10.1029/2018JC013967>.

Gao, W., Zhang, X., Yang, L., Liu, H., 2010. An improved sobel edge detection. In: *2010 3rd International Conference on Computer Science and Information Technology*, vol. 5, pp. 67–71. <http://dx.doi.org/10.1109/ICCSIT.2010.5563693>.

Gomes, E.R., Mulligan, R.P., Brodie, K.L., McNinch, J.E., 2016. Bathymetric control on the spatial distribution of wave breaking in the surf zone of a natural beach. *Coast. Eng.* 116, 180–194. <http://dx.doi.org/10.1016/j.coastaleng.2016.06.012>, URL <https://www.sciencedirect.com/science/article/pii/S0378383916301235>.

Gomes da Silva, P., Coco, G., Garnier, R., Klein, A.H., 2020. On the prediction of runup, setup and swash on beaches. *Earth-Sci. Rev.* 204, 103148. <http://dx.doi.org/10.1016/j.earscirev.2020.103148>, URL <https://www.sciencedirect.com/science/article/pii/S0012825219306828>.

Guimarães, P.V., Farina, L., Toldo, E., Diaz-Hernandez, G., Akhmatskaya, E., 2015. Numerical simulation of extreme wave runup during storm events in Tramandai Beach, Rio Grande do Sul, Brazil. *Coast. Eng.* 95, 171–180. <http://dx.doi.org/10.1016/j.coastaleng.2014.10.008>, URL <https://www.sciencedirect.com/science/article/pii/S0378383914001963>.

Harley, M., 2017. Coastal storm definition. In: *Coastal Storms*. John Wiley and Sons, Ltd, pp. 1–21. <http://dx.doi.org/10.1002/9781118937099.ch1>, arXiv:<https://onlinelibrary.wiley.com/doi/pdf/10.1002/9781118937099.ch1>.

Henderson, C.S., Fiedler, J.W., Merrifield, M.A., Guza, R., Young, A.P., 2022. Phase resolving runup and overtopping field validation of SWASH. *Coast. Eng.* 175, 104128. <http://dx.doi.org/10.1016/j.coastaleng.2022.104128>, URL <https://www.sciencedirect.com/science/article/pii/S0378383922000436>.

Holland, K., Holman, R., Lippmann, T., Stanley, J., Plant, N., 1997. Practical use of video imagery in nearshore oceanographic field studies. *IEEE J. Ocean. Eng.* 22 (1), 81–92. <http://dx.doi.org/10.1109/48.557542>.

Holland, K.T., Raubenheimer, B., Guza, R.T., Holman, R.A., 1995. Runup kinematics on a natural beach. *J. Geophys. Res.: Oceans* 100 (C3), 4985–4993. <http://dx.doi.org/10.1029/94JC02664>, arXiv:<https://agupubs.onlinelibrary.wiley.com/doi/pdf/10.1029/94JC02664>.

Holman, R.A., 1986. Extreme value statistics for wave run-up on a natural beach. *Coast. Eng.* 9 (6), 527–544. [http://dx.doi.org/10.1016/0378-3839\(86\)90002-5](http://dx.doi.org/10.1016/0378-3839(86)90002-5).

Holman, R.A., Brodie, K.L., Spore, N.J., 2017. Surf zone characterization using a small quadcopter: Technical issues and procedures. *IEEE Trans. Geosci. Remote Sens.* 55 (4), 2017–2027. <http://dx.doi.org/10.1109/TGRS.2016.2635120>.

Holman, R., Haller, M.C., 2013. Remote sensing of the nearshore. *Ann. Rev. Mar. Sci.* 5, 95–113. <http://dx.doi.org/10.1146/annurev-marine-121211-172408>.

- Holman, R.A., Holland, K.T., Lalejini, D.M., Spansel, S.D., 2011. Surf zone characterization from unmanned aerial vehicle imagery. *Ocean Dyn.* 61 (11), 1927–1935. <http://dx.doi.org/10.1007/s10236-011-0447-y>.
- Holman, R.A., Lalejini, D.M., Edwards, K., Veeramony, J., 2014. A parametric model for barred equilibrium beach profiles. *Coast. Eng.* 90, 85–94. <http://dx.doi.org/10.1016/j.coastaleng.2014.03.005>, URL <https://www.sciencedirect.com/science/article/pii/S0378383914000581>.
- Holman, R., Plant, N., Holland, T., 2013. CBathy: A robust algorithm for estimating nearshore bathymetry. *J. Geophys. Res.: Oceans* 118 (5), 2595–2609. <http://dx.doi.org/10.1002/jgrc.20199>.
- Kalman, R.E., 1960. A new approach to linear filtering and prediction problems. *J. Basic Eng.* 82 (1), 35–45. <http://dx.doi.org/10.1115/1.3662552>, arXiv:https://asmedigitalcollection.asme.org/fluidsengineering/article-pdf/82/1/35/5518977/35_1.pdf.
- Kanopoulos, N., Vasanthavada, N., Baker, R., 1988. Design of an image edge detection filter using the Sobel operator. *IEEE J. Solid-State Circuits* 23 (2), 358–367. <http://dx.doi.org/10.1109/4.996>.
- Klein, A.H.d.F., Short, A.D., Bonetti, J., 2016. Santa Catarina beach systems. In: *Brazilian Beach Systems*. In: Coastal Research Library, vol. 17, Springer International Publishing, pp. 465–506.
- Komar, P., 1997. *Beach Processes and Sedimentation*, 2nd Revised ed. Prentice Hall, New Jersey, p. 554. <http://dx.doi.org/10.1201/9781351072908>.
- Lange, A.M., Fiedler, J.W., Becker, J.M., Merrifield, M.A., Guza, R., 2022. Estimating runup with limited bathymetry. *Coast. Eng.* 172, 104055. <http://dx.doi.org/10.1016/j.coastaleng.2021.104055>, URL <https://www.sciencedirect.com/science/article/pii/S0378383921001940>.
- Ma, C., Gao, W., Yang, L., Liu, Z., 2010. An improved sobel algorithm based on median filter. In: *2010 2nd International Conference on Mechanical and Electronics Engineering*, vol. 1, pp. V1–88–V1–92. <http://dx.doi.org/10.1109/ICMEE.2010.5558590>.
- Matheen, N., Harley, M.D., Turner, I.L., Splinter, K.D., Simmons, J.A., Thran, M.C., 2021. Bathymetric data requirements for Operational Coastal Erosion forecasting using XBeach. *J. Mar. Sci. Eng.* 9 (10), <http://dx.doi.org/10.3390/jmse9101053>, URL <https://www.mdpi.com/2077-1312/9/10/1053>.
- Medellín, G., Brinkkemper, J.A., Torres-Freyermuth, A., Appendini, C.M., Mendoza, E.T., Salles, P., 2016. Run-up parameterization and beach vulnerability assessment on a barrier Island: A downscaling approach. *Nat. Hazards Earth Syst. Sci.* 16 (1), 167–180. <http://dx.doi.org/10.5194/nhess-16-167-2016>, URL <https://nhess.copernicus.org/articles/16/167/2016/>.
- Nicolae Lerma, A., Pedreros, R., Robinet, A., Sénéchal, N., 2017. Simulating wave setup and runup during storm conditions on a complex barred beach. *Coast. Eng.* 123, 29–41. <http://dx.doi.org/10.1016/j.coastaleng.2017.01.011>, URL <https://www.sciencedirect.com/science/article/pii/S0378383916301284>.
- Nicolae Lerma, A., Pedreros, R., Senechal, N., 2016. Wave set-up and run-up variability on a complex barred beach during highly dissipative storm conditions. *J. Coast. Res.* (75 (10075)), 882–886. <http://dx.doi.org/10.2112/SI75-177.1>, arXiv:<https://meridian.allenpress.com/jcr/article-pdf/doi/10.2112/SI75-177.1/1315761/si75-177.1.pdf>.
- Pazini, K.C., Bonetti, J., da Silva, P.G., Klein, A.H.F., 2022. Spotting areas critical to storm waves and surge impacts on coasts with data scarcity: A case study in Santa Catarina, Brazil. *Nat. Hazards* 112 (3), 2493–2521. <http://dx.doi.org/10.1007/s11069-022-05275-1>.
- Renka, R.J., 1988. Multivariate interpolation of large sets of scattered data. *ACM Trans. Math. Softw.* 14 (2), 139–148.
- Ruggiero, P., Holman, R.A., Beach, R.A., 2004. Wave run-up on a high-energy dissipative beach. *J. Geophys. Res.: Oceans* 109 (C6), <http://dx.doi.org/10.1029/2003JC002160>, arXiv:<https://agupubs.onlinelibrary.wiley.com/doi/pdf/10.1029/2003JC002160>.
- Rutten, J., Torres-Freyermuth, A., Puleo, J.A., 2021. Uncertainty in runup predictions on natural beaches using XBeach nonhydrostatic. *Coast. Eng.* 166 (February), 103869. <http://dx.doi.org/10.1016/j.coastaleng.2021.103869>.
- Senechal, N., Abadie, S., Gallagher, E., MacMahan, J., Masselink, G., Michallet, H., Reniers, A., Ruessink, G., Russell, P., Sous, D., Turner, I., Arduin, F., Bonneton, P., Bujan, S., Capo, S., Certain, R., Pedreros, R., Garlan, T., 2011a. The ECORS-Truc Vert'08 nearshore field experiment: Presentation of a three-dimensional morphologic system in a macro-tidal environment during consecutive extreme storm conditions. *Ocean Dyn.* 61 (12), 2073–2098. <http://dx.doi.org/10.1007/s10236-011-0472-x>.
- Senechal, N., Coco, G., Bryan, K.R., Holman, R.A., 2011b. Wave runup during extreme storm conditions. *J. Geophys. Res.: Oceans* 116 (C7), <http://dx.doi.org/10.1029/2010JC006819>, arXiv:<https://agupubs.onlinelibrary.wiley.com/doi/pdf/10.1029/2010JC006819>.
- Silveira, L.F., Klein, A.H.F., Tessler, M.G., 2011. Classificação morfodinâmica de praias do estado de Santa Catarina e do litoral Norte do estado de São Paulo Utilizando Sensoriamento Remoto. *Braz. J. Aquatic Sci. Technol.* 15 (2), 13–28.
- SMC, 2011. Sistema de modelagem costeira: Manual do usuário SMC-brasil. p. 160, URL http://smcbrasil.ihcantabria.com/wp-content/uploads/2013/06/Manual_SMC_v3.0.pdf.
- Stockdon, H.F., Holman, R.A., Howd, P.A., Sallenger, A.H., 2006. Empirical parameterization of setup, swash, and runup. *Coast. Eng.* 53 (7), 573–588. <http://dx.doi.org/10.1016/j.coastaleng.2005.12.005>.
- Stokes, K., Poate, T., Masselink, G., King, E., Saulter, A., Ely, N., 2021. Forecasting coastal overtopping at engineered and naturally defended coastlines. *Coast. Eng.* 164, 103827. <http://dx.doi.org/10.1016/j.coastaleng.2020.103827>, URL <https://www.sciencedirect.com/science/article/pii/S0378383920305135>.
- Valentini, N., Saponieri, A., Danisi, A., Pratola, L., Damiani, L., 2019. Exploiting remote imagery in an embayed sandy beach for the validation of a runup model framework. *Estuar. Coast. Shelf Sci.* 225, 106244. <http://dx.doi.org/10.1016/j.ecss.2019.106244>, URL <https://www.sciencedirect.com/science/article/pii/S0272771418310333>.
- Virtanen, P., Gommers, R., Oliphant, T.E., Haberland, M., Reddy, T., Cournapeau, D., Burovski, E., Peterson, P., Weckesser, W., Bright, J., van der Walt, S.J., Brett, M., Wilson, J., Millman, K.J., Mayorov, N., Nelson, A.R.J., Jones, E., Kern, R., Larson, E., Carey, C.J., Polat, İ., Feng, Y., Moore, E.W., VanderPlas, J., Laxalde, D., Perktold, J., Cimrman, R., Henriksen, I., Quintero, E.A., Harris, C.R., Archibald, A.M., Ribeiro, A.H., Pedregosa, F., van Mulbregt, P., SciPy 1.0 Contributors, 2020. SciPy 1.0: Fundamental algorithms for scientific computing in Python. *Nat. Methods* 17, 261–272. <http://dx.doi.org/10.1038/s41592-019-0686-2>.
- Vos, K., 2017. *Remote Sensing of the Nearshore Zone Using a Rotary-Wing UAV (Ph.D. thesis)*. Ecole Polytechnique Federale De Lausanne, TX, USA, p. 84.
- Vousdoukas, M., Perakakis, P., Idrissi, S., Vila, J., 2012. SVMF: A MATLAB toolbox for stereo-vision motion tracking of motor reactivity. *Comput. Methods Programs Biomed.* 108 (1), 318–329. <http://dx.doi.org/10.1016/j.cmpb.2012.01.006>, URL <https://www.sciencedirect.com/science/article/pii/S0169260712000338>.
- Wright, L., Short, A., 1984. Morphodynamic variability of surf zones and beaches: A synthesis. *Mar. Geol.* 56 (1), 93–118. [http://dx.doi.org/10.1016/0025-3227\(84\)90008-2](http://dx.doi.org/10.1016/0025-3227(84)90008-2), URL <https://www.sciencedirect.com/science/article/pii/0025322784900082>.
- Yates, M.L., Guza, R.T., O'Reilly, W.C., 2009. Equilibrium shoreline response: Observations and modeling. *J. Geophys. Res.: Oceans* 114 (C9), <http://dx.doi.org/10.1029/2009JC005359>, arXiv:<https://agupubs.onlinelibrary.wiley.com/doi/pdf/10.1029/2009JC005359>.
- Zijlema, M., Stelling, G., Smit, P., 2011. SWASH: An operational public domain code for simulating wave fields and rapidly varied flows in coastal waters. *Coast. Eng.* 58 (10), 992–1012. <http://dx.doi.org/10.1016/j.coastaleng.2011.05.015>.